660–669 Nucleic Acids Research, 2012, Vol. 40, No. 2 Published online 29 September 2011
doi:10.1093/nar/gkr781

The human histone chaperone sNASP interacts with linker and core histones through distinct mechanisms

Huanyu Wang[1], Zhongqi Ge[1], Scott T. R. Walsh[2,*] and Mark R. Parthun[1,*]

[1]Department of Molecular and Cellular Biochemistry, The Ohio State University, Columbus, OH 43210 and [2]Institute for Bioscience and Biotechnology Research, Department of Cell Biology and Molecular Genetics, University of Maryland College Park, 9600 Gudelsky Drive, Rockville, MD 20850, USA

Received April 29, 2011; Revised September 2, 2011; Accepted September 5, 2011

ABSTRACT

Somatic nuclear autoantigenic sperm protein (sNASP) is a human homolog of the N1/N2 family of histone chaperones. sNASP contains the domain structure characteristic of this family, which includes a large acidic patch flanked by several tetratricopeptide repeat (TPR) motifs. sNASP possesses a unique binding specificity in that it forms specific complexes with both histone H1 and histones H3/H4. Based on the binding affinities of sNASP variants to histones H1, H3.3, H4 and H3.3/H4 complexes, sNASP uses distinct structural domains to interact with linker and core histones. For example, one of the acidic patches of sNASP was essential for linker histone binding but not for core histone interactions. The fourth TPR of sNASP played a critical role in interactions with histone H3/H4 complexes, but did not influence histone H1 binding. Finally, analysis of cellular proteins demonstrated that sNASP existed in distinct complexes that contained either linker or core histones.

INTRODUCTION

The assembly of chromatin structure requires a precise and ordered assembly of core and linker histones with genomic DNA. This is a fundamental process in eukaryotic cells that allows for the enormous degree of compaction that is necessary for eukaryotic genomes to be packaged inside the nucleus and ensures that both short-term and long-term transcriptional programs are properly regulated and epigenetically transmitted. Proteins known as histone chaperones play a key role in chromatin assembly. Most histone chaperones bind to a specific subset of histones, regulate aspects of histone sub-cellular dynamics and often mediate the transfer of histones to DNA during the formation of a nucleosome (1–3).

Based on sequence and structural similarity, histone chaperones can be grouped into several families (4–6). One is the N1/N2 family of histone chaperones. This family is based on the *Xenopus laevis* N1/N2 proteins that were originally isolated from frog oocytes. *Xenopus* oocytes store a large amount of histone proteins in preparation for events that occur post-fertilization. The N1/N2 proteins form a complex with the histone H3/H4 complexes that are stored in these oocytes. N1/N2 then participates in assembling histone H3 and H4 into chromatin during the rapid rounds of cell division that occur following fertilization (7–9).

The N1/N2 family histone chaperones contain a conserved domain structure that consists of four tetratricopeptide repeats (TPRs) with the second TPR interrupted by the insertion of a large domain that is highly enriched in acidic amino acids (Figure 1A) (10). TPR domains typically mediate protein–protein interactions and fold into two anti-parallel α-helices (11,12). Analysis of COOH-terminal deletions of the Xenopus N1/N2 protein indicated that the acidic domain and a large hydrophobic region that includes the third and fourth TPRs contribute to core histone binding (12).

Evidence now indicates that N1/N2 family histone chaperones are involved in more aspects of chromatin biology than just the storage of H3/H4 complexes in oocytes. N1/N2 homologs have been identified in fungal species where histone storage is not likely to be a relevant function. For example, in *Saccharomyces cerevisiae*, Hif1p has been shown to be an H3/H4-specific chaperone that associates with the Hat1p-containing type B histone acetyltransferase complex that is involved in the acetylation of newly synthesized histone H4 (13,14). In addition, the N1/

*To whom correspondence should be addressed. Tel: +614 292 6215; Fax: +614 292 4118; Email: Parthun.1@osu.edu
Correspondence may also be addressed to Scott Walsh. Tel: +240 314 6478; Fax: +240 314 6225; Email: swalsh12@umd.edu

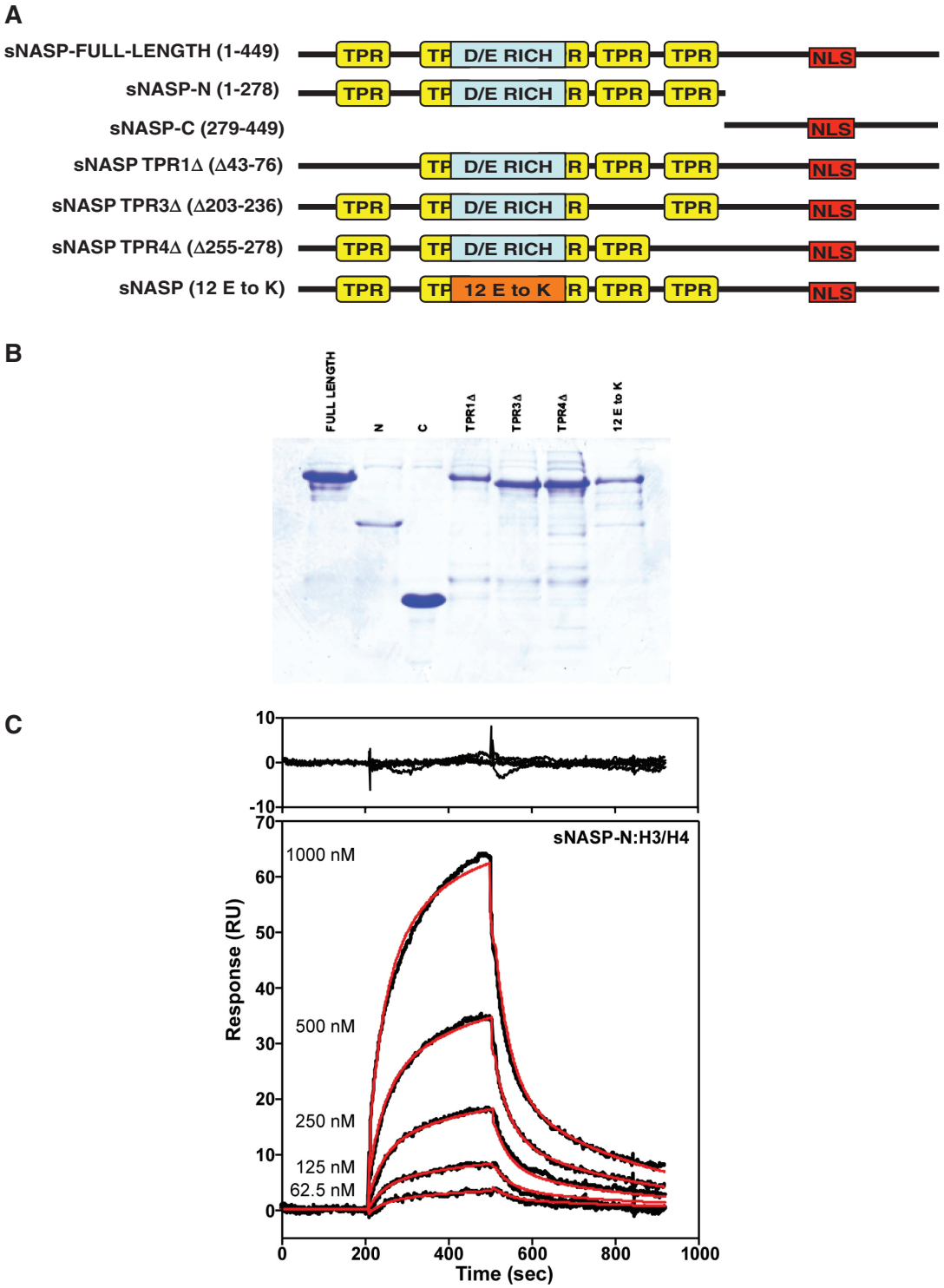

Figure 1. Mutational analysis of sNASP histone binding specificity. (**A**) Schematic diagrams of the sNASP variants. Each of the constructs also contains an NH_2-terminal His-tag. (**B**) For the biochemical assays, the sNASP constructs were expressed from *E. coli*, purified by Ni^{2+}-chelate chromatography and resolved by SDS–PAGE using Coomassie blue staining. Proteins were visualized by Coomassie blue staining. (**C**) Surface plasmon resonance (SPR) binding sensorgrams displayed for various concentrations of sNASP-N injected over a H3.3/H4 tetramer sensor chip (black lines). The data were globally fit to a 1:1 Langmuir binding model (red lines) and the residuals plotted above the kinetics plot. For SPR measurements, the sNASP variants were further purified over a size-exclusion chromatography (SEC) column described in the 'Materials and Methods' section.

N2 homolog in *Schizosaccharomyces pombe*, Sim3p, has been found to be involved in the assembly of the centromeric histone H3 variant (10).

The mammalian homologs of N1/N2 are known as NASP (nuclear autoantigenic sperm protein)(15). NASP is found as two differentially spliced isoforms. The longer form is known as testicular NASP (tNASP) and the smaller form is somatic NASP (sNASP). The tNASP form can be found in the testis, embryonic tissues and some transformed cells. sNASP appears to be expressed in all dividing cells (16). NASP plays an essential role in mammals as demonstrated by the early embryonic lethality of a mouse knockout model (17). In addition, RNAi knockdown experiments in human tissue culture cells indicate that NASP is important for cell cycle progression (17). Also, NASP is a DNA damage-dependent target of the ATM/ATR checkpoint kinases and siRNA experiments indicate that NASP is necessary for proper DNA damage repair (18).

Despite its obvious similarity with the N1/N2 proteins, sNASP was originally identified as a linker histone-specific chaperone (16). In fact, sNASP displays binding affinity to histone H3/H4 complexes and to histone H1 (19,20). To understand the mechanisms that underlie this unique binding specificity, a critical issue to resolve is whether the binding of sNASP to linker and core histones is linked or whether these interactions occur independently. Through a targeted mutational analysis, we determined that sNASP interacts with linker and core histones through distinct structural domains. In addition, characterization of cellular sNASP indicates association with linker and core histones occurs in the context of distinct complexes. Therefore, sNASP may play a central role in coordinating the dynamics of both core and linker histones.

MATERIALS AND METHODS

Plasmid DNA construction

The full-length human sNASP (449 amino acids), which contains a six-residue histidine tag (His-tag) at the NH_2-terminus, was produced in *Escherichia coli* as described previously (19). Six mutant constructs of sNASP were generated. TPR1Δ, TPR3Δ and TPR4Δ were generated by the partial overlapping PCR method. Primers were designed to be complementary to the sequences flanking the regions that were targeted for deletion: sNASP-TPR1Δ (deleted residues 43–76), TPR3Δ (deleted residues 203–236) and TPR4Δ (deleted residues 255–278) motifs. The upstream primer partially overlaps with the downstream primer to prevent primer self-complementarity. PCR products were then subjected to endonuclease Dpn-1 digestion to remove template DNA and propagated in *E. coli*. DH10β competent cells were used for DNA sequencing and further analysis. sNASP-12E/K was generated by site-directed mutagenesis from pDEST17/sNASP using the Quikchange protocol (Stratagene). The DNA fragments that encoded NH_2- (sNASP-N, residues 1–278) or COOH-termini (sNASP-C, residues 279–449) and flanking attB sequences were generated by PCR and then introduced into donor vector pDONR 221 by the BP recombination reaction. After being propagated and verified, the donor clones containing the desired gene sequences were subjected to LP recombination reactions and subsequently cloned into destination vector pDEST-17. All sNASP constructs were confirmed by DNA sequencing. In addition, mutant constructs were introduced into destination vector pT-REX-DEST 31 (Invitrogen) which allows the expression in mammalian cells. As with the *E. coli* expressed proteins, these constructs also contain an NH_2-terminal His-tag that allows for visualization and protein purification.

Protein expression and purification

Plasmids that contain sequences including full-length sNASP and its mutants were each transformed into *E. coli* BL21 AI competent cells to allow for L-arabinose-inducible expression. Protein expression and subsequent purification (see Figure 1B) was performed following procedures as described (19).

Surface plasmon resonance

The sNASP variants were further purified using size-exclusion chromatography (SEC) over a Superdex S-300 16/60 column equilibrated with 25 mM Tris–HCl, pH 7.0, 300 mM NaCl, 0.1 mM EDTA and 0.05% NP-40. A similar protocol was used to purify full-length sNASP in our previous study (19). Recombinant human histones $H1^0$, H3.3 and H4 were purchased from New England Biolabs and used without further purification. Histones H3.3 and H4 were incubated overnight at room temperature in the supplied buffer to form the tetramer. The H3.3/H4 complex was purified over a Superdex 200 10/300 GL SEC column using the above buffer. Surface plasmon resonance (SPR) experiments were performed using a Biacore 3000 instrument (GE Healthcare) at 25°C. The histones were coupled to CM5 sensor chips and experiments were performed as previously described (19). The binding sensorgrams were pooled, trimmed and fit as previously described (19). The binding constants were derived from data performed in triplicate.

Cell culture and transfections

U2OS cells that were engineered for tetracycline-inducible expression were cultured in McCoy's media supplemented with 10% FBS at 37°C in 5% CO_2 supply. The U2OS cells were transfected with pT-REX-DEST 31 plasmids (Invitrogen) carrying the His-tag full-length sNASP or mutants using the Fugene reagent kit (Roche). Stably transfected clones were selected against 200 μg/ml G418. Stable clones that can be induced by tetracycline were confirmed by western blot.

Whole cell extracts and *in vivo* pull down

Cells ($2\text{-}4 \times 10^7$ cells/ml) were collected 24 h after tetracycline induction. Cells were washed once with PBS and then frozen with liquid nitrogen. After being thawed on ice, cell pellets were resuspended in an equal volume of whole cell extract buffer (25% glycerol, 420 mM NaCl, 1.5 mM $MgCl_2$, 0.2 mM EDTA. 20 mM HEPES pH 7.6 and

0.1% Triton X-100) and incubated on ice for 20 min. After incubation, they were pelleted again. The supernatants were saved as whole cell extracts. Whole cells extracts from cells expressing full-length sNASP or its mutants were incubated with 50 µL Ni^{2+}-NTA beads (settled volume, Qiagen) for 2 h at 4°C. Beads were washed five times with wash buffer (50 mM $NaPO_4$ pH 7.5, 300 mM NaCl, 10% Glycerol, 10 mM Imidazole and 0.05% NP-40). Bound proteins were eluted with SDS dye followed by boiling. Western blotting was used to determine bound proteins. Anti-histone antibodies were obtained from Abcam and anti-NASP antibody was as described previously (19).

Co-immunoprecipitation

Mouse anti-H1 antibody (Abcam) was immobilized with coupling gel from ProFound™ Mammalian Co-immunoprecipitation Kit (Pierce, Rockford, IL). Eighty microliters of coupling gel was incubated with 500 µl of elution fraction from the full-length sNASP pull down. The gel was then washed six times with 1 ml of 1× PBS to remove unbound protein. Bound proteins were eluted by boiling in 80 µl of 2× SDS loading dye (0.12 M Tris–HCl, pH 6.8, 4% SDS, 20% glycerol, 0.002% bromophenol blue and 5% β-mercaptoethanol). The bound proteins were resolved by SDS–PAGE and detected by western blot analysis.

Size exclusion chromatography of sNASP complexes

The elution fraction (0.250 ml) from the full-length sNASP pull down was applied to a size exclusion chromatography (SEC) column (10 × 300 mm Superose 6 column, GE Healthcare) equilibrated with buffer consisting of 25 mM Tris (pH 7.0), 0.1 mM EDTA, 10% glycerol and 50 mM NaCl. The column was run at a flow rate of 0.30 ml/min and 0.25 ml fractions were collected. The elution profiles of proteins were determined by western blot analysis.

RESULTS

A variety of *in vitro* biochemical approaches have shown that sNASP forms high-affinity complexes with both histone H1 and histone H3/H4 complexes (19,20). However, how these binding affinities relate to the association of sNASP with histones *in vivo* has not been well characterized. For example, there may be distinct pools of sNASP, one of which is bound to histone H1 and a second that is bound to histones H3/H4. The binding of H1 and H3/H4 could be mutually exclusive and, thus, these histones could compete for binding to NASP. Alternatively, these separate pools could function independently to regulate linker and core histone dynamics. Another possibility is that sNASP may simultaneously bind to a combination of H1, H3, H4 and H3/H4 complexes. These sNASP/H1/H3/H4 complexes might then be involved in the coordinated assembly of core and linker histones.

sNASP interacts with linker and core histones through distinct domains

As a first step in determining how sNASP interacts with different histone populations, we have generated a series of deletion mutations of sNASP to identify the specific domains responsible for binding to the linker and core (H3.3, H4 and H3.3/H4 tetramer) histones. We have designed, expressed and purified a series of sNASP constructs that created targeted deletions and mutations to localize the binding activities of sNASP to specific domains of the protein (Figure 1A and B). These constructs included an NH_2-terminal fragment that included all four TPR repeats and the acidic domain (sNASP-N, residues 1–278), a COOH-terminal fragment that started after the final TPR repeat and included the nuclear localization sequence (NLS, sNASP-C, residues 279–449), individual deletions of the three intact TPR repeats (TPR1 Δ, TPR3 Δ and TPR4 Δ) and a mutant in which 12 of the glutamic acid residues in the acidic domain were changed to lysine residues (sNASP-12 E/K). The acidic domain mutant was constructed in this way for a number of reasons. First, attempts to delete the acidic domain were unsuccessful as these proteins were unstable in *E. coli*. Second, the acidic domain contains 21 glutamic acid residues and 7 aspartic acid residues with many of the glutamic acid residues clustered together to form patches of negative charge. We mutated these clusters in such a way as to eliminate the long contiguous stretches of acidic residues. In addition, the glutamic acid residues chosen for mutation spanned the length of the acidic domain. Finally, we chose to convert the glutamic acid residues to lysine as these are roughly isosteric changes that, while reversing the charge of the residue, retain the potential for surface charges that may be important for protein folding.

Quantitative binding studies of the interactions of the sNASP variants to human histones $H1^0$, H3.3, H4 and H3.3/H4 tetramers were measured using SPR. We have included the uncomplexed histones H3.3 and H4 in this analysis as it is not clear whether the association of sNASP with the core histones occurs only after the formation of H3/H4 dimers or tetramers. For example, the association of N1 family histone chaperones with Hat1 histone acetyltransferase complexes occurs at an early step in the chromatin assembly pathway that may precede H3/H4 complex formation (13,21). Therefore, sNASP may interact with surfaces on individual histones that are not available in histone complexes. An example of a SPR binding sensorgram for the sNASP-N:H3.3/H4 interaction is given in Figure 1C and the binding constants listed in Table 1. Full-length sNASP binds to histone $H1^0$ with k_{on} and k_{off} rates of $1.54 \times 10^4\,M^{-1}\,s^{-1}$ and $1.48 \times 10^{-4}\,s^{-1}$, respectively. The calculated binding affinity ($K_d = k_{off}/k_{on}$) for this interaction is 9.6 nM. Full-length sNASP interacts with H3.3 with a k_{on} of $1.68 \times 10^3\,M^{-1}\,s^{-1}$ and a k_{off} of $1.58 \times 10^{-3}\,s^{-1}$ giving a K_d of 940 nM. Full-length sNASP binds to H4 with an ~4-fold higher K_d of 236 nM ($k_{on} = 3.01 \times 10^3\,M^{-1}\,s^{-1}$ and $k_{off} = 7.10 \times 10^{-4}\,s^{-1}$) in comparison to the sNASP:H3.3 interaction. Finally, full-length sNASP binds to H3.3/H4 tetramers with a k_{on} of $4.47 \times 10^3\,M^{-1}\,s^{-1}$ and

Table 1. SPR binding constants of NASP variants to human histones $H1^0$, H3.3, H4, and H3/H4 tetramer[a]

	k_{on} ($M^{-1}s^{-1}$)	k_{off} (s^{-1})	K_d (nM)[b]	var/wt[c]
H1 binding				
sNASP	$1.54\ (3) \times 10^4$	$1.48\ (2) \times 10^{-4}$	9.6 ± 0.2	1
SNASP-N	$4.86\ (4) \times 10^4$	$8.91\ (9) \times 10^{-4}$	18.3 ± 0.3	1.9
sNASP-C	ND[d]	ND	NB[e]	NB
SNASP-12E/K	$2.25\ (4) \times 10^1$	$6.77\ (10) \times 10^{-4}$	$30.1 \pm 5.6\,\mu M$	3100
TPR1Δ	$2.86\ (4) \times 10^3$	$8.58\ (12) \times 10^{-4}$	300 ± 6.0	31
TPR3Δ	$3.37\ (2) \times 10^4$	$1.45\ (2) \times 10^{-3}$	43.0 ± 0.7	4.5
TPR4Δ	$1.51\ (1) \times 10^4$	$2.17\ (7) \times 10^{-4}$	14.4 ± 0.5	1.5
H3.3 binding				
sNASP	$1.68\ (3) \times 10^3$	$1.58\ (1) \times 10^{-3}$	940 ± 16	1
SNASP-N	$3.37\ (29) \times 10^4$	$2.01\ (2) \times 10^{-3}$	59.6 ± 0.8	0.063
sNASP-C	ND	ND	NB	NB
SNASP-12E/K	$1.24\ (8) \times 10^2$	$4.69\ (6) \times 10^{-4}$	3780 ± 270	4.0
TPR1Δ	$1.01\ (17) \times 10^4$	$3.01\ (7) \times 10^{-3}$	298 ± 8.1	0.32
TPR3Δ	$3.66\ (65) \times 10^4$	$1.96\ (2) \times 10^{-3}$	53.6 ± 1.3	0.057
TPR4Δ	$3.03\ (31) \times 10^4$	$6.52\ (2) \times 10^{-4}$	21.5 ± 0.7	0.023
H4 binding				
sNASP	$3.01\ (3) \times 10^3$	$7.10\ (8) \times 10^{-4}$	236 ± 3.3	1
sNASP-N	$1.86\ (18) \times 10^4$	$2.14\ (1) \times 10^{-3}$	115 ± 1.2	2.1
SNASP-C	ND	ND	NB	NB
SNASP-12E/K	$1.70\ (11) \times 10^3$	$7.64\ (4) \times 10^{-4}$	449 ± 3.8	1.9
TPR1Δ	$2.75\ (34) \times 10^3$	$1.17\ (1) \times 10^{-3}$	425 ± 6.5	1.8
TPR3Δ	$1.37\ (57) \times 10^3$	$2.35\ (2) \times 10^{-3}$	1720 ± 73	7.3
TPR4Δ	$3.24\ (47) \times 10^3$	$1.47(1) \times 10^{-3}$	454 ± 7.9	1.9
H3.3/H4 tetramer binding				
sNASP	$4.47\ (83) \times 10^3$	$2.16\ (3) \times 10^{-3}$	483 ± 88	1
sNASP-N	$4.43\ (6) \times 10^3$	$5.50\ (2) \times 10^{-3}$	1240 ± 18	2.6
sNASP-C	ND	ND	NB	NB
SNASP-12E/K	$1.56\ (8) \times 10^3$	$8.33\ (7) \times 10^{-4}$	534 ± 5.1	1.1
TPR1Δ	$3.65\ (40) \times 10^2$	$1.55\ (1) \times 10^{-3}$	4250 ± 440	8.8
TPR3Δ	$4.47\ (10) \times 10^3$	$1.99\ (3) \times 10^{-3}$	445 ± 12	0.9
TPR4Δ	$1.52\ (40) \times 10^1$	$1.85\ (2) \times 10^{-3}$	$122 \pm 6\,\mu M$	250

Values in parentheses are the standard deviation of the mean of standard errors in the final

[a]SPR experiments were performed in 25 mM Tris–HCl, pH 7.0, 0.3 M NaCl, 0.1 mM EDTA, and 0.05% NP-40 at 25.0 ± 0.1°C.

[b]$K_d = k_{off}/k_{on}$.

[c]Var/wt = $K_d$variant/$K_d$wild-type.

[d]ND, Not determined.

[e]NB, No detectable binding at concentrations used.

a k_{off} of $2.16 \times 10^{-3}\,s^{-1}$ resulting in a K_d of 483 nM. The K_ds of full-length sNASP for human $H1^0$ and H3.3/H4 tetramers are within a factor of 2 compared with our previous SPR results measuring the binding interactions of full-length sNASP to bovine H1 and chicken H3/H4 tetramers (19). These results highlight the broad cross-species binding affinities of human sNASP to linker and core histones that were either isolated from natural sources or recombinantly expressed and purified. It is interesting to note that the binding affinity of the sNASP:H3.3/H4 tetramer interaction falls in between the binding affinities observed for the individual sNASP:H3.3 and sNASP:H4 core histone interactions. The full-length sNASP rate constants to human $H1^0$, H3.3, H4 and H3.3/H4 tetramers serve as reference points to compare the mutations made in the domain structure of sNASP.

While the COOH-terminal fragment of sNASP was unable to bind to any of the histones, the NH_2-terminal fragment of sNASP (sNASP-N) bound to histone $H1^0$ with an affinity approaching that of the full-length sNASP (1.9-fold weaker). The binding of sNASP-N to H4 or H3.3/H4 tetramers was reduced approximately 2- and 3-fold, respectively. Surprisingly, the sNASP-N interaction to H3.3 has ~16-fold higher binding affinity than the full-length sNASP:H3.3 interaction. The changes in K_ds of sNASP-N to the histones occur through faster on- and off-rate constants with the exception of the sNASP-N:H3.3/H4 on rate. These results suggest that the COOH-terminus of sNASP contributes equally to core and linker histone binding, but with an overall minor effect. The exception is with H3.3 where the COOH-terminus has a negative impact on this interaction.

We were able to further localize the domains of sNASP that are involved in linker and core histone interactions. The TPR1 domain contributed more for H1 binding than core histone binding as deletion of this domain resulted in a 31-fold decrease in binding affinity to H1, while only a 8.8-fold decrease was observed for the H3.3/H4 complexes (Table 1). The TPR1 domain exhibited only a 1.8-fold decrease when removed for the H4 interaction, but its' removal resulted in a 3-fold increase in binding affinity for the H3.3 interaction. A similar trend was observed for the TPR3 domain of sNASP with it being more important for H1 binding (4.8-decrease upon removal) than the H3.3/H4 tetramer, which had a similar binding affinity relative to full-length sNASP. In addition, the TPR3 domain of sNASP has a positive influence on the interaction with histone H4 (7.3-fold decrease) and a negative influence for the interaction with histone H3.3 (18-fold increase relative to the full-length sNASP interaction).

Importantly, we also identified residues and domains that play a critical role in the binding to specific histone types. In this respect, two sNASP mutants were particularly informative, sNASP 12 E/K and sNASP TPR4Δ. The affinity of sNASP 12 E/K for histone H1 decreased >3000-fold while its affinities for H3.3/H4 tetramers, H4 or H3.3 were nearly unchanged or moderately changed (1.1-, 1.9- or 4.0-fold decrease, respectively). Conversely, deletion of the fourth TPR repeat domain (sNASP TPR4Δ) had a dramatic effect on H3.3/H4 tetramer affinity (250-fold decrease) with small 1.5- and 1.9-fold effects on histone H1 and H4 binding affinities. These results suggest that sNASP uses distinct residues, domains and/or mechanisms to interact with the individual linker and core histones and aggregated species (H3.3/H4 tetramer or dimer).

Binding of sNASP to linker and core histones *in vivo*

To determine whether the effect of the sNASP mutations on histone binding in the cell matched with the *in vitro* results, we constructed a set of cell lines (derived from U2OS cells) that expressed these mutations. Of note, the U2OS cells express various isoforms of the linker and H3 histones. As with the bacterially expressed proteins, these sNASP constructs also contained an NH_2-terminal six-residue histidine tag (His-tag) that allowed for protein isolation. Whole cell extracts were made from cells expressing the sNASP constructs indicated in Figure 1A. The His-tag sNASP protein in these extracts was then bound to Ni^{2+}-chelate chromatography columns. Following washing, the bound proteins were eluted with imidazole. As expected, full-length sNASP bound histones H1, H3 and H4 (Figure 2). It is interesting to note that very little

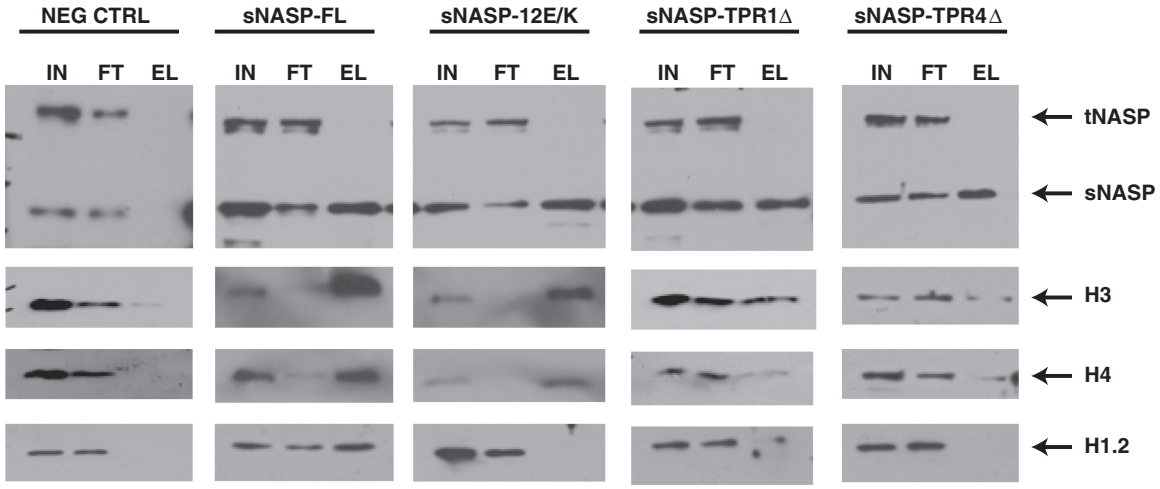

Figure 2. Binding of sNASP to histones *in vivo*. U2OS cell lines were isolated that allow for the Tet-inducible expression of His-tag full-length sNASP or various mutant forms of sNASP (as indicated at the top of each column). Whole cell extracts were made from each cell line and passed through a Ni^{2+}-chelate affinity column. After extensive washing, proteins bound to the column were eluted with buffer containing a high concentration of imidazole. An aliquot of the whole cell extract (IN, 10%), the flow-through fraction (FT, 10%) and bound (elution) fraction (EL, 25%) were resolved by SDS–PAGE and analyzed by western blot probed with the antibodies indicated to the right of the blots.

histone H3 and H4 were found in the flow-through fraction. As these whole cell extracts contain non-chromatin-associated proteins, this observation was consistent with previous reports that suggest that a significant fraction of the soluble H3 and H4 in cells is bound to sNASP-containing complexes (21–24). The sNASP 12E/K mutant displayed a similar level of interaction with H3 and H4 but no longer bound to histone H1. This agrees with the *in vitro* result where this mutant was specifically defective in histone H1 binding (Table 1). Also in agreement with the *in vitro* results, the sNASP TPR1Δ displayed diminished binding to both H3/H4 and H1. The sNASP TPR4Δ mutant, which was defective in H3/H4 binding *in vitro*, displayed little binding to these histones *in vivo*. Surprisingly, this mutant also showed a significant loss histone H1 binding. While the binding of sNASP mutants to linker and core histones in the cell were, in general, qualitatively similar to that observed for the recombinant sNASP constructs, it is important to note that the analysis of native complexes is not quantitative. The interaction between sNASP and histones in the cell occurs in the context of numerous other factors that are interacting with both sNASP and the histones. Therefore, the mutations in sNASP are likely to influence both the direct interactions with the histones and also the interactions with the other present *in vivo*.

sNASP is found in distinct complexes containing either linker or core histones

The observation that the binding of sNASP to H1 and H3/H4 involved separable domains raises the important issue of whether sNASP interacts with linker and core histones independently or whether it can bind simultaneously to both types of histone. To address this question, we used gel filtration chromatography (Superose 6) to resolve native sNASP-containing complexes present in the elution fraction from the full-length sNASP Ni^{2+}-chelate column pull down. Comparing the elution profiles of sNASP, core histones and linker histone provided information on the distribution of the histones in specific sNASP-containing complexes. As seen in Figure 3A, the bulk of the sNASP eluted in a fairly broad peak that was centered at ~150 kDa (peaked at fraction 58). The majority of the histone H1 (H1.2) was found in a narrower peak, centered on fraction 62, which overlapped with part of the sNASP peak. Based on the elution position where sNASP and histone H1.2 overlapped, this complex had an apparent molecular weight <150 kDa. The remainder of the sNASP peak co-eluted with histone H4. The elution of the sNASP/H4 overlap indicated an apparent molecular weight for this complex ≥150 kDa. Intriguingly, there was no apparent overlap in the peaks of H4 and H1.2. We did observe that a small fraction of the H1.2 and H4 eluted together in a very high-molecular-weight complex (fraction 28). This complex may be due to a low level of contaminating chromatin as we also observed a trace of histone H2B that eluted only in this fraction. The size exclusion chromatography results suggested that, while sNASP is associated with both core and linker histones, there is little or no sNASP that is simultaneously bound to both types of histone.

To confirm the size exclusion chromatography results, we also performed a co-immunoprecipitation experiment in which the elution fraction from the Ni^{2+}-chelate column containing full-length sNASP was incubated with antibodies directed against histone H3. If sNASP exists in complexes containing H3, H4 and H1, we would expect that immunoprecipitation of histone H3 would also pull down sNASP, histone H4 and histone H1. However, as seen in Figure 3B, only sNASP and histone H4 were co-immunoprecipitated with the histone H3. An analogous co-immunoprecipitation experiment using α-histone H1 antibodies was uninformative as there was a significant level of non-specific interaction between the α-H1

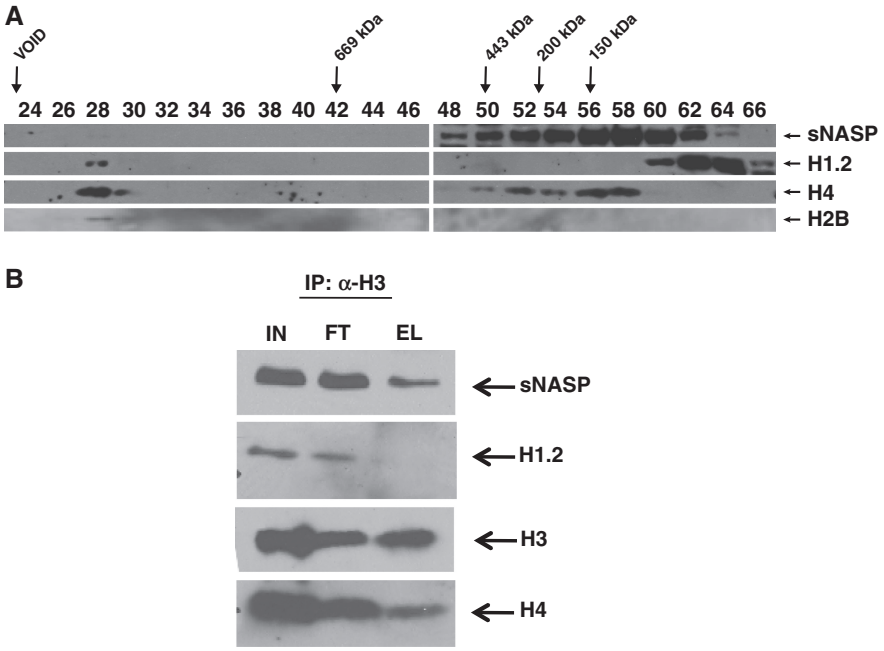

Figure 3. sNASP can bind to linker and core histones simultaneously. (**A**) The Ni^{2+}-chelate column elution fraction isolated from the full-length sNASP whole cell extract was resolved by size exclusion chromatography (Superose 6). The indicated fractions were analyzed by western blots and probed using antibodies that recognized sNASP, histone H1.2, histone H4 and histone H2B (as marked). Arrows on the top of the blots indicate the void volume and elution position of molecular weight standards. (**B**) The Ni^{2+}-chelate column elution fraction isolated from the full-length sNASP whole cell extract shown in Figure 2 was immunoprecipitated with an α-H3 antibody. The input flow-through and bound fractions were analyzed as described in Figure 2.

antibodies and sNASP. These observations are consistent with the results of the size exclusion chromatography and indicate that sNASP was found in distinct complexes that contain either core or linker histones but not in complexes that included both histone types simultaneously.

DISCUSSION

Binding specificity is a signature characteristic of histone chaperones. sNASP possesses a unique specificity in that it binds with high affinity to both histone H1 and histone H3/H4 complexes. One important question that we have addressed is whether the binding to discreet types of histones occurs through a common mechanism. The observation that different domains are necessary for the interaction between sNASP and core or linker histones strongly suggests that distinct mechanisms underlie its binding to different classes of histone.

Currently, there are no crystal or solution structures for any of the N1/N2 family members or complexes with histones. To provide a structural template to map the domain mutagenesis study of sNASP for its interaction with the histones, we submitted the primary sequence of full-length sNASP to the Robetta server using default parameters and it generated a *de novo* structural model using the Rosetta algorithm developed by Baker and co-workers (25).

Figure 4 displays the structural model of full-length sNASP. The predicted sNASP structure has an extended topology that can be broken into an NH_2- and COOH-terminal lobes connected by a coiled-coil domain (CCD). The NH_2-terminal lobe is structurally larger than the COOH-terminal lobe. The predicted structure consists of large amounts of α-helical secondary consistent with circular dichroism measurements (20). Primary sequence algorithm predicts residues 281–323 with high probability to form a CCD (26). TPR1 does not adopt a classical TPR fold, but has extended packing against other α-helices in the NH_2-terminal lobe. TPR3 and TPR4 do fold into TPR motifs packing against each other and parts of the NH_2-terminal lobe and the CCD. SEC (Figure 3) (20,21) and analytical ultracentrifugation (20,21) experiments indicate the quaternary structure of sNASP to be a dimer with a K_d of 100 nM. Rosetta built only a monomer, but with the extended structure of this model, we posit the dimer interface localizes to the CCD (residues 281–323) in a similar fashion as the structure of NAP-1 dimer determined by Luger and co-workers (27). The sNASP structural model provides a visual representation to map our domain mutational study with high confidence.

The computationally derived structure of sNASP has several attractive features that correlate well with our mutational study and with previous data regarding linker and core histone interactions with sNASP. First, the COOH-terminus of the sNASP structural is separated in distance from the NH_2-terminus and our mutational data here demonstrated that this region was not critical for the interaction of sNASP with either linker or core histones or previously for nucleosome assembly (28), whereas the NH_2-terminus lobe to residue 322 was essential. Second,

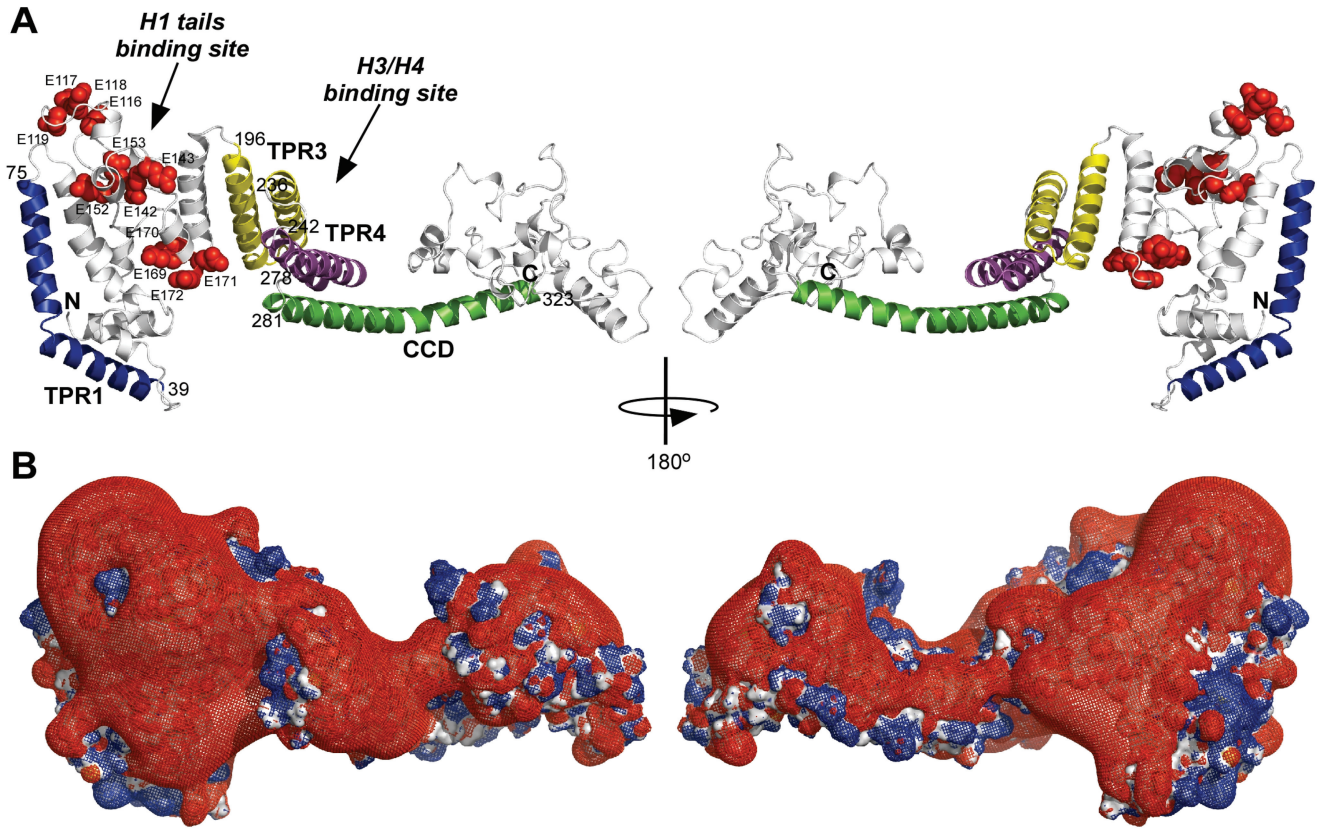

Figure 4. Structural model of a sNASP monomer generated by Rosetta (25). (**A**) Ribbon representation of sNASP highlighting the TPR motifs (TPR1 in blue from residues 39–75, TPR3 in yellow from residues 196–236, and TRP4 in purple from residues 242–278), coiled-coil domain (CCD in green from residues 281–323), and the glutamates residues, drawn as CPK models, mutated to lysines in the sNASP-12E/K construct. The NH_2- and COOH-termini are labeled accordingly. The predicted binding sites of the linker and core histone sites are indicated. (**B**) The linear Poisson–Boltzman equation was solved for sNASP using APBS (30) with 150 mM monovalent salt at 25° C. The solvent accessible surfaces areas are displayed and colored blue (+5 kT/e) and red (−5 kT/e). The electrostatic potential gradient for sNASP is displayed as a blue (+2 kT/e) and red mesh (−2 kT/e). Predicted structures and electrostatic potentials were viewed and rendered using PyMOL (31). The ribbon and electrostatic diagrams are oriented in the same manner and the two structural views are related by an 180° rotation around the vertical axis.

the deletion mutations of sNASP indicate that H1 binding localizes primarily to an acidic domain (residues 116–172), whereas the core histones localize to the regions around TPR3 and TPR4. The linker and core binding sites on the sNASP structural model are also distant from each other. Crystal structural determinations of free sNASP and sNASP complexes with H1 and H3/H4 are underway. Given that we do not observe sNASP complexes that contain both linker and core histones, it will be interesting to determine whether binding to one type of histone causes structural alterations that preclude simultaneous binding to the other. It should be noted that studies demonstrated that it was the tails, not the winged helix domain, of H1 that interact with sNASP (20).

Given the overall negatively charged sNASP molecule (isoelectric point, pI, of 4.35) and highly positively charged molecules of the linker and core histones (pIs ranging from 10.8 to 11.4), favorable electrostatics are large components of their binding associations. Calculation of the linear Poisson–Boltzmann equation (at 150 mM salt and 25°C) using the predicted sNASP structure highlights the large negative surface area and field potential around the NH_2-lobe localizing to the acidic insertion in TPR2 (30). This acidic domain was more important for the binding of sNASP to histone H1 than H3/H4 as determined using the sNASP-12E/K mutation. The sNASP-12E/K mutation increased the pI from 4.35 of wild-type sNASP to 4.72. These data suggest that the sNASP:H1 association is largely driven by more favorable electrostatic interactions than the sNASP:H3/H4 associations. A model whereby more favorable electrostatics drives the sNASP–H1 interaction could resolve some previously contradictory observations. Despite the fact that recombinant sNASP binds to histone H1 with a significantly higher affinity than to H3/H4, chromatography-based methods only detect the association of sNASP with H3/H4. For example, histone H1 is not retained on Ni^{2+}-chelate resin in the presence of recombinant His-tag sNASP. Also, recombinant sNASP and histone H1 do not co-purify during size exclusion chromatography (19). However, these columns are run in buffers containing a relatively high ionic strength (300 mM NaCl) to prevent non-specific binding of the purified histones to the column resins. Therefore, if the sNASP-H1 binding were primarily based on ionic

interactions, these are likely to be disrupted by the salt concentration of the buffer systems, which would then prevent detection of complex formation.

The fourth TPR repeat domain is essential for the interaction of sNASP with histone H3/H4 complexes. TPR repeats are found in many proteins and often mediate protein–protein interactions (11). TPR repeats have not previously been shown to mediate specific interactions with histones. However, a TPR repeat domain of SMYD3, a lysine methyltransferase that can specifically methylate histone H3 lysine 4, has been proposed to form a large part of the substrate binding site for this enzyme (29).

The binding stoichiometries of sNASP in its interactions with linker and core histones remain a difficult and open-ended question. The most definitive data regarding binding stoichiometries of sNASP to H3.1/H4 were measured using sedimentation equilibrium experiments using analytical ultracentrifugation (SE-AUC) (21). The SE-AUC data fit to a complicated binding equilibrium of sNASP:H3.1:H4 in molar ratios of 1:1:1 (38.5%), 2:2:2 (44.9%) and 1:2:2 (16.6%) (21). The SE-AUC experiments cannot distinguish between a monomer/dimer of sNASP binding to a H3.1/H4 dimer or a H3.1/H4 tetramer (21). A similar complication would exist using SE-AUC experiments by adding another component of the linker histone H1. Our size exclusion chromatography results are consistent with the possibility that native sNASP also exists as dimers but the resolution of this technique is not sufficient to make a definitive determination. If the cellular sNASP is present as dimers, our results suggest that these sNASP dimers are homomeric with respect to their histone substrates. That is, the lack of overlap between H1 and H4 in the sNASP complexes indicates that heteromeric complexes where one sNASP molecule is associated with histone H1 and the other is associated with H3/H4 may not exist at significant levels.

When combined, our results suggest a model of sNASP–histone interactions where sNASP exists in multiple states. The size exclusion chromatography observation that histone H1 and histone H4 overlap with distinct parts of this sNASP peak but do not overlap with each other suggests that there are discreet pools of sNASP that are associated with either histone H1 or histone H3/H4. These sNASP complexes may serve as a reservoir for newly synthesized (or newly displaced) histones prior to chromatin assembly. These sNASP complexes might then directly interact other factors involved in chromatin assembly as the histones are directed into specific assembly pathways (3,21). This model is consistent with the role of N1/N2 in the storage of histones in *Xenopus* oocytes as well as with the association of the *S. cerevisiae* homolog of sNASP, Hif1p, with the type B histone acetyltransferase Hat1p that is involved in the acetylation of newly synthesized histones (7,9,13). The ability of sNASP to associate with both linker and core histones places this histone chaperone in a position to play a critical role in coordinating the assembly of higher order chromatin structure.

ACKNOWLEDGEMENTS

We would like to thank Dr Dan Schoenberg for the kind gift of Tet-inducible U2OS cells. S.T.R.W. and M.R.P. dedicate this work in memory of Dr. Jonathan Widom, a valued colleague and friend.

FUNDING

The National Institutes of Health (GM62970 to M.R.P.) and a Pelotonia Predoctoral Fellowship from the Ohio State University Comprehensive Cancer Center (to Z.G.). Funding for open access charge: The National Institutes of Health (GM62970).

Conflict of interest statement. None declared.

REFERENCES

1. Ransom,M., Dennehey,B.K. and Tyler,J.K. (2010) Chaperoning histones during DNA replication and repair. *Cell*, **140**, 183–195.
2. Corpet,A. and Almouzni,G. (2009) Making copies of chromatin: the challenge of nucleosomal organization and epigenetic information. *Trends Cell. Biol.*, **19**, 29–41.
3. Das,C., Tyler,J.K. and Churchill,M.E. (2010) The histone shuffle: histone chaperones in an energetic dance. *Trends Biochem. Sci.*, **35**, 476–489.
4. Park,Y.J. and Luger,K. (2006) Structure and function of nucleosome assembly proteins. *Biochem Cell. Biol.*, **84**, 549–558.
5. De Koning,L., Corpet,A., Haber,J.E. and Almouzni,G. (2007) Histone chaperones: an escort network regulating histone traffic. *Nat. Struct. Mol. Biol.*, **14**, 997–1007.
6. Eitoku,M., Sato,L., Senda,T. and Horikoshi,M. (2008) Histone chaperones: 30 years from isolation to elucidation of the mechanisms of nucleosome assembly and disassembly. *Cell Mol. Life Sci.*, **65**, 414–444.
7. Kleinschmidt,J.A., Fortkamp,E., Krohne,G., Zentgraf,H. and Franke,W.W. (1985) Co-existence of two different types of soluble histone complexes in nuclei of Xenopus laevis oocytes. *J. Biol. Chem.*, **260**, 1166–1176.
8. Kleinschmidt,J.A., Dingwall,C., Maier,G. and Franke,W.W. (1986) Molecular characterization of a karyophilic, histone-binding protein: cDNA cloning, amino acid sequence and expression of nuclear protein N1/N2 of Xenopus laevis. *EMBO J.*, **5**, 3547–3552.
9. Dilworth,S.M., Black,S.J. and Laskey,R.A. (1987) Two complexes that contain histones are required for nucleosome assembly *in vitro*: role of nucleoplasmin and N1 in Xenopus egg extracts. *Cell*, **51**, 1009–1018.
10. Dunleavy,E.M., Pidoux,A.L., Monet,M., Bonilla,C., Richardson,W., Hamilton,G.L., Ekwall,K., McLaughlin,P.J. and Allshire,R.C. (2007) A NASP (N1/N2)-related protein, Sim3, binds CENP-A and is required for its deposition at fission yeast centromeres. *Mol. Cell*, **28**, 1029–1044.
11. D'Andrea,L.D. and Regan,L. (2003) TPR proteins: the versatile helix. *Trends Biochem. Sci.*, **28**, 655–662.
12. Kleinschmidt,J.A. and Seiter,A. (1988) Identification of domains involved in nuclear uptake and histone binding of protein N1 of Xenopus laevis. *EMBO J.*, **7**, 1605–1614.
13. Ai,X. and Parthun,M.R. (2004) The nuclear Hat1p/Hat2p complex: a molecular link between type B histone acetyltransferases and chromatin assembly. *Mol. Cell*, **14**, 195–205.
14. Poveda,A., Pamblanco,M., Tafrov,S., Tordera,V., Sternglanz,R. and Sendra,R. (2004) Hif1 is a component of yeast histone acetyltransferase B, a complex mainly localized in the nucleus. *J. Biol. Chem.*, **279**, 16033–16043.
15. O'Rand,M.G., Richardson,R.T., Zimmerman,L.J. and Widgren,E.E. (1992) Sequence and localization of human

NASP: conservation of a Xenopus histone-binding protein. *Dev. Biol.*, **154**, 37–44.
16. Richardson,R.T., Batova,I.N., Widgren,E.E., Zheng,L.X., Whitfield,M., Marzluff,W.F. and O'Rand,M.G. (2000) Characterization of the histone H1-binding protein, NASP, as a cell cycle-regulated somatic protein. *J. Biol. Chem.*, **275**, 30378–30386.
17. Richardson,R.T., Alekseev,O.M., Grossman,G., Widgren,E.E., Thresher,R., Wagner,E.J., Sullivan,K.D., Marzluff,W.F. and O'Rand,M.G. (2006) Nuclear autoantigenic sperm protein (NASP), a linker histone chaperone that is required for cell proliferation. *J. Biol. Chem.*, **281**, 21526–21534.
18. Matsuoka,S., Ballif,B.A., Smogorzewska,A., McDonald,E.R. 3rd, Hurov,K.E., Luo,J., Bakalarski,C.E., Zhao,Z., Solimini,N., Lerenthal,Y. *et al.* (2007) ATM and ATR substrate analysis reveals extensive protein networks responsive to DNA damage. *Science*, **316**, 1160–1166.
19. Wang,H., Walsh,S.T. and Parthun,M.R. (2008) Expanded binding specificity of the human histone chaperone NASP. *Nucleic Acids Res.*, **36**, 5763–5772.
20. Finn,R.M., Browne,K., Hodgson,K.C. and Ausio,J. (2008) sNASP, a histone H1-specific eukaryotic chaperone dimer that facilitates chromatin assembly. *Biophys J.*, **95**, 1314–1325.
21. Campos,E.I., Fillingham,J., Li,G., Zheng,H., Voigt,P., Kuo,W.H., Seepany,H., Gao,Z., Day,L.A., Greenblatt,J.F. *et al.* (2010) The program for processing newly synthesized histones H3.1 and H4. *Nat. Struct. Mol. Biol.*, **17**, 1343–1351.
22. Tagami,H., Ray-Gallet,D., Almouzni,G. and Nakatani,Y. (2004) Histone H3.1 and H3.3 complexes mediate nucleosome assembly pathways dependent or independent of DNA synthesis. *Cell*, **116**, 51–61.
23. Lewis,P.W., Elsaesser,S.J., Noh,K.M., Stadler,S.C. and Allis,C.D. (2010) Daxx is an H3.3-specific histone chaperone and cooperates with ATRX in replication-independent chromatin assembly at telomeres. *Proc. Natl Acad. Sci. USA*, **107**, 14075–14080.
24. Drane,P., Ouararhni,K., Depaux,A., Shuaib,M. and Hamiche,A. (2010) The death-associated protein DAXX is a novel histone chaperone involved in the replication-independent deposition of H3.3. *Genes Dev.*, **24**, 1253–1265.
25. Das,R. and Baker,D. (2008) Macromolecular modeling with rosetta. *Annu. Rev. Biochem.*, **77**, 363–382.
26. Lupas,A., Van Dyke,M. and Stock,J. (1991) Predicting coiled coils from protein sequences. *Science*, **252**, 1162–1164.
27. Park,Y.J. and Luger,K. (2006) The structure of nucleosome assembly protein 1. *Proc. Natl Acad. Sci. USA*, **103**, 1248–1253.
28. Osakabe,A., Tachiwana,H., Matsunaga,T., Shiga,T., Nozawa,R.S., Obuse,C. and Kurumizaka,H. Nucleosome formation activity of human somatic nuclear autoantigenic sperm protein (sNASP). *J. Biol. Chem.*, **285**, 11913–11921.
29. Xu,S., Wu,J., Sun,B., Zhong,C. and Ding,J. (2011) Structural and biochemical studies of human lysine methyltransferase Smyd3 reveal the important functional roles of its post-SET and TPR domains and the regulation of its activity by DNA binding. *Nucleic Acids Res.*, **39**, 4438–4449.
30. Baker,N.A., Sept,D., Joseph,S., Holst,M.J. and McCammon,J.A. (2001) Electrostatics of nanosystems: application to microtubules and the ribosome. *Proc. Natl Acad. Sci. USA*, **98**, 10037–10041.
31. DeLano,W. (2002) The PyMOL Molecular Graphics System.